Chapter 4

Air Shower Measurement Techniques

The Auger Observatory will employ methods of analysis of air showers which have been developed by prior experiments. The results from past and present surface arrays and air fluorescence detectors were reviewed in the last chapter. Here we describe the details of the methods of these experiments. The next chapter will give detailed expectations for the performance of the Auger systems.

The manner in which the essential physics of air showers affects the data is discussed first, with emphasis on how the direction, energy, and nature of the primary particle are obtained from analysis both of the particles at the ground and of the air fluorescence or scintillation. Next, details of surface array methods is given. We conclude with an examination of the basis and implementation of the air fluorescence technique.

4.1 Properties and Development of Air Showers

The goal of the Auger Observatory is to study the arrival direction, energy, and primary mass composition of cosmic rays. The fluorescence detector and surface array provide complementary methods of extracting this information from the showers. Each relies on a combination of signal timing and amplitude measurements to characterize the geometry of the shower. Energy is measured calorimetrically in the fluorescence detector, and by sampling the particle density at ground level in the surface detector. The depth of shower maximum and the shape of the longitudinal profile provide composition diagnostics for the fluorescence data. In the surface detector, composition information is extracted from a number of shower characteristics which reflect the depth of shower maximum and the muon content of the shower.

Before proceeding to discuss in greater detail how each of these quantities is determined, it is useful to review key characteristics of air showers with emphasis on those aspects which impact the measured quantities most directly. When it is relevant, special emphasis is placed on ground array measurements made using water Čerenkov detectors, these having been selected for the Auger Observatory.

4.1.1 The Electromagnetic and Muon Components

An air shower is a particle cascade initiated by the interaction of an energetic cosmic ray high in the atmosphere. If the primary cosmic ray particle is a nucleon or nucleus, the cascade begins with a hadronic interaction. The number of hadrons increases through subsequent generations of particle interactions. In each generation, however, about 30% of the energy is transferred to an electromagnetic cascade by the rapid decays of π^0 mesons. Ultimately, the electromagnetic cascade dissipates roughly 90% of the primary particle's energy through ionization. The remaining energy is carried by muons and neutrinos from charged pion decays. Figure 4.1 illustrates the development of an air shower in schematic form.

The energy dissipated by the electromagnetic component of the shower, and hence the total number of low energy electromagnetic particles in the cascade, is very nearly proportional to the shower energy. However, the total number of muons reaching the ground grows more slowly with primary energy, mainly because of the transferral of energy from the hadronic interaction channels into electromagnetic showering. This effect is important for distinguishing air showers produced by heavy nuclear primaries from those of protons or light nuclei. Simulations predict [127] that the total number of muons reaching the ground in a proton induced air shower increases with primary energy as $E^{0.85}$. As a consequence, viewing a nucleus with atomic number A as a collection of individual nucleons each with energy E/A, the number of muons in a shower induced by that nucleus is related to the number of muons in a proton shower (of the same total energy) by

$$N_\mu^A = A^{0.15} N_\mu^p.$$

Thus, an iron shower (A=56) will have about 80% more muons than a proton shower with the same E. These effects will be described more fully below (section 4.2.3).

Because fluorescence is essentially a calorimetric technique, it is primarily sensitive to the electromagnetic component of the shower. On the other hand, signals from water Čerenkov detectors, such as those planned for use in the Auger Observatory surface array, have comparable contributions from the muon and electromagnetic components.

4.1.2 Spatial Structure of the Shower

An air shower is a broad, thin disc of particles moving at the speed of light through the atmosphere. The particles ionize and excite N_2 molecules in the air, causing radiation of near-UV photons. From a distance, the fluorescence detector sees the shower as a spot of light whose motion is along the *shower axis* or *core*. The intensity of the light, corrected for geometrical and atmospheric effects, reflects the longitudinal development of the shower, and its integral is proportional to the energy deposited in the atmosphere.

An air shower's *depth of maximum* (X_{max}) is the location in the atmosphere where the shower has developed the largest number of particles. X_{max} depends on both the total energy and the mass of the primary nucleus. At the same total energy, an air shower from a heavy nucleus is expected to develop faster than a shower initiated by a proton. This is

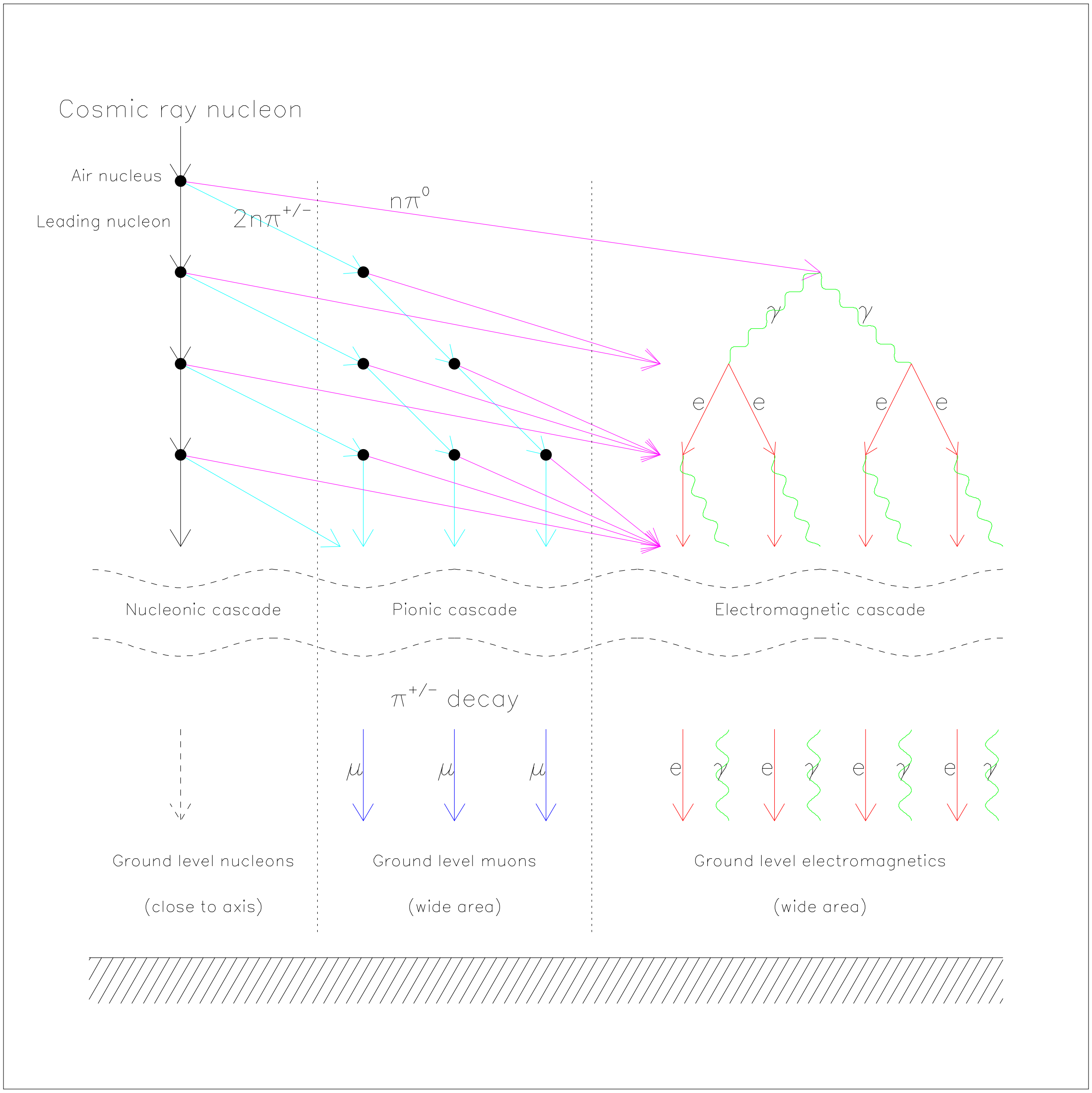

Figure 4.1: Schematic diagram showing the principal EAS cascade processes. An incident cosmic ray nucleon is assumed, and the resulting shower divided into three categories; the nucleonic cascade consisting of the surviving primary itself in the guise of a "leading-nucleon", the pionic cascade, and the electromagnetic cascade which is fed by neutral pion decay. This picture is, of course, highly simplified.

partly because a heavy nucleus has a larger cross section, so it tends to interact sooner than a proton. More importantly, however, the heavy nucleus behaves much like a superposition of its constituent nucleons. The *superposition model* is a simple and very good estimator of the average behavior of many shower properties. An iron nucleus produces an air shower which can be approximated as the superposition of 56 nucleon showers, each with 1/56th of the iron nucleus' energy. X_{max} for proton showers increases by at least 55 g/cm^2 for each decade of energy, so reducing the energy by 1/56 decreases the expected X_{max} by approximately 100 g/cm^2. An iron shower therefore has an expected X_{max} about 100 g/cm^2 less than the expected X_{max} for a proton shower of the same energy.

The particle swarm is spreads away from the shower axis due to the combined effects of multiple Coulomb scattering and the transverse momentum in interactions and decays. The particles spread out laterally from the shower axis in a pancake-like shower front which can be detected over a large area when it strikes the ground. The highest particle density is near the axis, falling off with distance on a scale determined by the Moliere radius in air (80 m at ground level). Outside the core region the distribution of particles is axially symmetric about the core. This is an experimental fact, confirmed over a wide range of energies (see Figure 3.1 in the last chapter, and Section 4.3.1 below). It is also predicted to be the case by shower simulations. The density of particles falls off rapidly with increasing core distance. It is customary to characterize the observed lateral distribution of showers at ground level by a *lateral distribution function*. A modified power law is normally used; the exact form and slope which is appropriate depends on the type of ground array detector which is employed, and the atmospheric depth at which observations are made.

The longitudinal profile of the most energetic air shower yet observed was shown in the last chapter as Figure 3.7. The left part of Figure 4.2 shows the lateral distributions of ground particles in a giant shower as predicted by simulation. (Details of the simulation procedures are given in the next chapter.) Close to the axis, low energy electrons and photons outnumber muons by several orders of magnitude. However, the muons have a flatter lateral distribution, and at large core distances carry significantly more energy per particle ($\sim$ GeV as opposed to $\sim$ 10 MeV for gammas and electrons). Also note that far from the core the electromagnetic cascade is dominated by photons.

Thin scintillators essentially measure charged particle density. Deep water Čerenkov detectors have a strong sensitivity to the more penetrating muons, and also convert most of the gamma rays into observable signal. To predict the actual lateral distribution which will be observed it is necessary to convolve the ground particle energy spectra at given core distance with the appropriate response curves for the detectors being used. This process is illustrated in the right part of Figure 4.2, where the signal observed in 1.2 m deep water detectors is plotted for each shower component together with the total. Notice that at large core distances ($>$ 1 km), the muons and electromagnetic particles make approximately equal contributions to the total signal from a water Čerenkov detector.

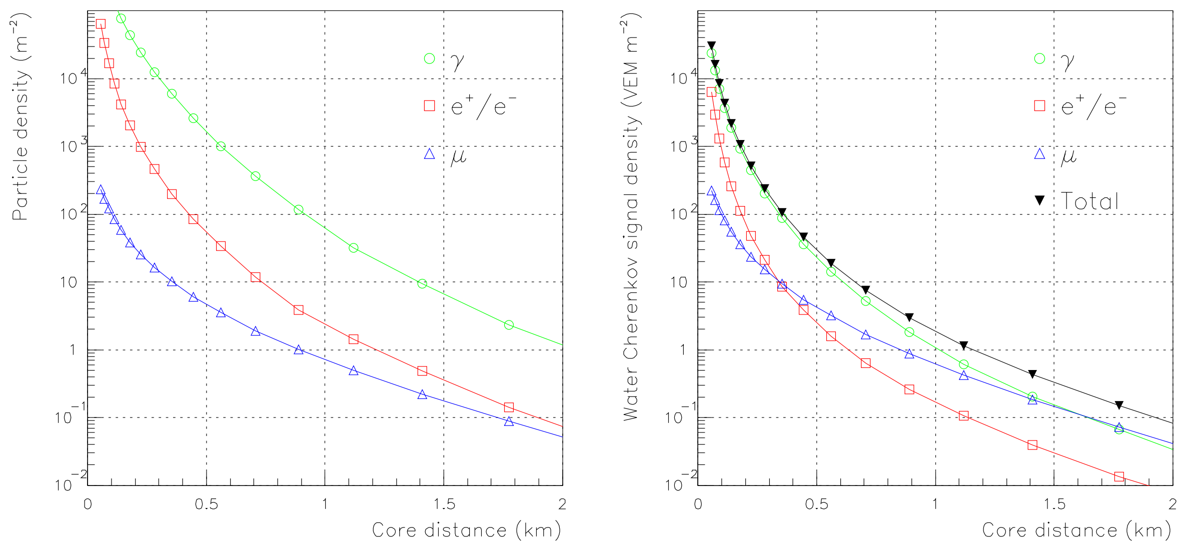

Figure 4.2: The left plot shows the simulated lateral distributions of the three main shower components at ground level for a 10^{19} eV proton shower. In the right frame the particles have been convolved with the response of a 1.2 m deep water Čerenkov detector, such as that proposed for the Auger Observatory.

4.1.3 Time Structure of the Shower Front

Particles scatter from the region of the shower axis throughout its development. The shower core effectively acts as a moving point source of both fluorescence photons and particles, which make their way to detectors far from the core. The plane tangent to the shower front at the axis is the *shower plane*. The shower front itself is slightly curved, resembling a cone. Particles far from the core will arrive behind the shower plane due to simple geometry.

Generally speaking, those particles arriving at the ground first at point some given distance from the core originated higher, and thus earlier, in the cascade (this can be simply seen by considering the geometry of path-length differences). Electrons and photons diffuse away from the shower axis throughout the shower development. Thus, far from the core particles are spread in time, with the time spread roughly proportional to the distance from the axis. This time spread helps to distinguish distant large showers from nearby small showers, and is thus useful in triggering the surface array. The time spread becomes greater as the depth of shower maximum increases.

Muons tend to arrive earlier than electrons and photons, because they suffer much less scattering and so have more direct paths to the ground. Iron showers, which are both muon-rich and have developed higher in the atmosphere relative to proton showers, thus have a signal which arrives over a shorter time than that from a proton shower with the same total energy. "Rise-time" measures based on this effect are among the most robust diagnostics of composition for the surface array.

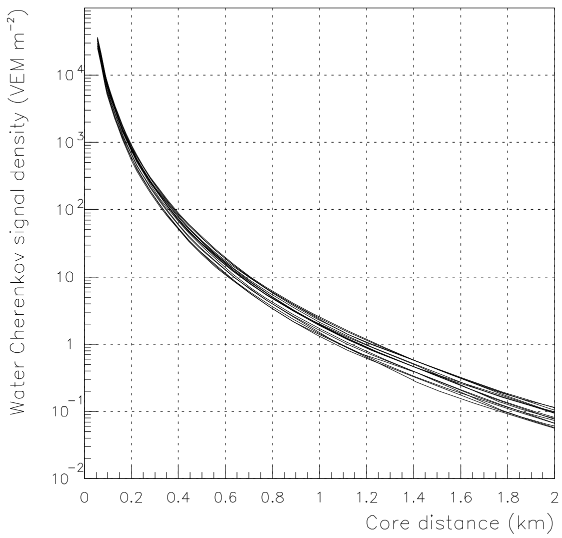

Figure 4.3: Lateral distributions of individually simulated proton air showers as observed in 1.2 m deep water Čerenkov detectors. A range of zenith angles ($\theta < 30°$), and energies ($10^{19} < E < 10^{20}$ eV) are included. Signal density is normalized by energy to 10^{19} eV.

4.1.4 Fluctuations in Shower Development

The most important source of fluctuations in shower development are the depth and characteristics of the first few interactions. Fluctuations in later interactions are averaged over a large number of particles and are not important. The depth of first interaction has a direct effect on the depth of shower maximum. Recalling Figure 2.8 in Chapter 2, variations in the total shower size at the ground result from roughly shifting the entire average profile higher or lower, depending on the depth of the starting point. In addition, fluctuations in the relative number of charged versus neutral pions in the first few generations of the cascade affect both the rate of development of the electromagnetic cascade and the muon content of the shower.

These physical fluctuations in the shower as observed at ground level have been estimated using MOCCA simulations. At the high energies of interest here, fluctuation in the muon component is approximately 15%, while the fluctuation in the electromagnetic component is only about 5% [124]. The fractional fluctuation in the ground particle density is roughly independent of radius beyond a few 100 m from the core. In water Čerenkov detectors, where the muon and electromagnetic components make comparable contributions to the signal, the physical fluctuation in the total signal is about 10%. Figure 4.3 shows the lateral distributions of a number of individually simulated showers over a range of zenith angles and energies, and with physical fluctuations included as presently understood.

4.2 Determination of Shower Parameters

4.2.1 The Shower Direction and Axis

"Geometrical reconstruction" is the important procedure of determining the shower axis and core location at the ground. The direction of the shower axis is the cosmic ray's arrival direction. If three ground stations record the shower, the shower direction can be computed by triangulation, finding the unique downward going speed-of-light shower front which accounts for the three positions and arrival times. When more than three stations trigger, a least squares method is used to find the plane front which fits best.

The position of the shower axis in space is located by exploiting the circular symmetry of particle densities in the shower plane (a plane perpendicular to the axis). This assumption of axial symmetry was mentioned in Section 4.1.2 above, and is the fundamental principle on which ground array analysis is based. For showers arriving close to the vertical the symmetry in the plane of the ground is of course circular; away from the zenith it becomes elliptical. A crude initial estimate of the position where the shower core impacts the ground is the "center of gravity" of the density measurements. Using the shower direction determined previously, and a given core impact position, the lateral distance of a detector can be calculated. Reconstruction proceeds by fitting the detector densities at their computed axial distances to an empirical *lateral distribution function*, the most probable core impact position and shower size being sought.

Once the core impact position has been determined it is possible to re-fit the detector times allowing for curvature of the shower front. This provides a refined shower direction, and the whole process can be repeated. After a small number of iterations (≤ 3) convergence is achieved. It is clearly key to this process that the lateral distribution function be well known. This is the case from previous experiments, whose results are also well reproduced by current Monte Carlo calculations — see Sections 4.3.1 and 5.2.4 for detailed discussion.

A better determination of the axis is achieved if the shower is also measured by the fluorescence detector. The axis is then constrained to lie in the plane containing the fluorescence detector and the viewing directions of the illuminated pixels. Locating the shower axis within that shower-detector plane is achieved using timing, both of the ground station detectors and of the spot of fluorescence light as it passes the various pixels. In this case the core impact position is located with minimal use of ground detector density information, and the lateral distribution can be studied in an essentially independent manner.

With or without the fluorescence detector, determination of the shower axis improves with the size of the shower. This is because greater numbers of particles (or UV photons for the fluorescence detector pixels) give a better measure of the passing shower front, and because more ground stations can be used in the fit. For measurements by the ground array alone, the typical angular resolution for vertical showers at 10^{19} eV is about $2°$, improving to $< 1°$ at 10^{20} eV. The error in the core impact position decreases from 80 m to 50 m. For hybrid measurements (fluorescence detector with ground array), the angular resolution improves from $0.25°$ to $0.20°$ over the same energy. The core position uncertainty decreases from 35 m to 20 m. (See the next chapter for details of these methods and results.)

4.2.2 Energy

The cascade of ionizing particles is monitored in the atmosphere via nitrogen fluorescence. The amount of light produced at each atmospheric depth is proportional to the shower *size*, i.e., the number of charged particles N_e. By measuring the light produced at many depths, the fluorescence detector determines the shower's longitudinal profile $N_e(X)$. The atmospheric depth X is measured in units of g/cm^2 along the shower axis. As the shower size increases, the original energy gets divided among more and more particles. The average energy eventually becomes low enough that ionizing particles are removed from the cascade, by ionization energy losses, at a rate exceeding their production rate by bremsstrahlung and pair production. The shower size therefore reaches its maximum size N_{max} at some atmospheric depth X_{max} (its *depth of maximum*), and the size decreases beyond that depth.

The integral of the longitudinal profile is a calorimetric measure of the total electromagnetic shower energy,

$$E_{em} = 2.2 \text{ MeV/g/cm}^2 \times \int N_e(X)\, dX,$$

since a charged particle in the cascade deposits an average of 2.2 MeV into the atmosphere in each depth interval of 1 g/cm^2 [118]. The portion of the electromagnetic cascade reaching the ground is included by fitting a functional form to the observed longitudinal profile and integrating that function past the surface depth.

This electromagnetic cascade energy is a lower bound for the energy of the primary cosmic ray. The amount of unmeasured energy which goes into the ground as muons and neutrinos depends on the shower development and is subject to fluctuations. For protons, the unmeasured energy is about 5% on average. For iron primaries, the mean is about 15%. The Fly's Eye analysis assumed a uniform 10% unmeasured energy. That gives no more than a 5% expected error for any nucleus and a 10% error for γ-rays. The energy not measured by the fluorescence detector can be estimated using the measured muon densities. (The measured X_{max} provides correlated information. Larger X_{max} at fixed electromagnetic energy implies less energy in muons and neutrinos, as will be discussed below with composition issues.) The fraction of primary energy not dissipated by the electromagnetic cascade can be estimated shower by shower by exploiting the ground array's muon information and the X_{max} measurement.

Ground arrays have traditionally determined the shower energy by interpolating and/or extrapolating the measurements to a single quantity which is known from shower simulations to correlate well with total energy for all primary particle types. The Haverah Park energies are based on energy correlation with $\rho(600)$, which is the signal density per square meter in water tanks at a distance of 600m from the shower core. The AGASA detector uses $S(600)$, the energy deposition density in plastic scintillators at 600 m from the core. The use of these energy estimators are well established. Extensive modeling by Hillas[114] and others[122] have shown that variations in shower physics models and mass composition affect the energy estimates only weakly. For the Haverah Park and AGASA arrays $\rho(600)$ and $S(600)$ can be found rather accurately, with uncertainties less than 20% (this includes roughly 10% physical fluctuation and 10% reconstruction uncertainty).

Because of the larger spacing between particle counters in the Auger ground array, it is more reliable to determine densities at 1.0 to 1.5 km from the core, rather than at 600 m. An important advantage of the Auger detector will be the separate measurements of muon density (mu) and the electromagnetic particle density (em) when measurements are made at sufficiently large distances from core that the individual muon pulses can be discerned. Algorithms to optimally identify these muon pulses as near to the core as possible are currently under development. The pair (mu,em) should be a more powerful indicator of energy than either density by itself or a combination of them such as $\rho(600)$. In addition, the ground array measures quantities such as the time distribution of the incoming particles, slope of the lateral distribution, and curvature of the shower front. These quantities are sensitive both to the muon fraction and to the depth of shower maximum, and will aid in both energy and primary mass reconstruction.

The hybrid data set will provide a distribution function in the multidimensional parameter space consisting of the fluorescence detector parameters E and X_{max}, and of the parameters measured by the ground array discussed above. Here E is the fluorescence detector's energy measurement (corrected for unmeasured energy based on its measured X_{max}). This allows the ground array to be inter-calibrated with the fluorescence detector, and enables the ground array to measure shower energy without reference to any hadronic interaction model or cascade simulation.

In the determination of shower energy, there are numerous advantages in the Auger detector's hybrid configuration. A shower measured in hybrid mode has an internal consistency check on the energy, since the ground array and the fluorescence detector independently measure the shower size at ground level. The fluorescence detector "trains" the ground array as explained in the previous paragraph, so the ground array can determine a shower's energy without the fluorescence detector and without reliance on any air shower development simulation. The ground array will also assist the fluorescence measurements. Many showers will be detected at large distances where atmospheric attenuation uncertainty can cause uncertainty in the longitudinal profile normalization. The array's measurement of shower size at ground level will provide the crucial normalization for those longitudinal profiles.

4.2.3 Primary Mass

The muon content of air showers is a powerful indicator of primary mass. The superposition model of a heavy nucleus can be invoked to explain why an iron shower produces more muons than a proton shower. The energy is divided among the constituent nucleons, so it takes fewer generations to distribute the hadronic energy into low energy pions which can decay before interacting. That means less energy is lost to the electromagnetic cascade, which results in more low energy pions than in a proton shower of the same energy. This is a general argument which pertains to all hadronic interaction models.

To evaluate quantitatively the relative muon production in heavy nucleus showers *vs.* proton showers, first note that muon production in proton showers increases with energy as $E^{0.85}$ [127]. The number of muons does not increase linearly with energy because more generations are required at higher energy to reduce the average pion energy down to where decay becomes likely. The extra generations mean a larger fraction of the energy is lost to the electromagnetic cascade, so a smaller fraction of the original energy gets delivered to those low energy pions which decay. Considering a nucleus-initiated shower as a superposition of A showers, each with energy E/A, we find that the total number of muons is

$$N_\mu^A \propto A(E/A)^{0.85},$$

or, comparing to proton showers,

$$N_\mu^A = A^{0.15} N_\mu^p.$$

Thus we expect that an iron shower ($A = 56$) will produce about 80% more muons than a proton shower of the same total energy.

The foregoing explanations for why X_{max} and muon number both correlate with primary mass may suggest that X_{max} and muon production are both controlled by the same shower development feature, so measuring both is redundant. To some extent that is the case. If a proton's primary collision were somehow to yield 56 equal-energy hadrons which all go on to interact, then its longitudinal profile should resemble the expected iron profile for the same total energy, and its muon content should be consistent with what is expected in an iron shower. In shower simulations, X_{max} and muon number are indeed correlated. But the correlation is far from perfect because of additional fluctuations which do not produce strongly correlated effects. For example, fluctuations in the number of charged *vs.* neutral pions in the first generation affect the number of low energy pions – hence muons – more than the shape of the electromagnetic longitudinal profile (e.g. X_{max}). While not independent, X_{max} and muon density are separate handles on composition. Moreover, they are measured with essentially independent instruments.

Similar remarks pertain to a third measurable quantity which correlates with the primary mass, the *rise-time* of the particle pulse far from the shower core. One practical example would be the time interval between the arrival of the 10% and 50% points of the integrated signal ($t_{10/50}$); other similar quantities are also used. Like X_{max} and muon density, its correlation with mass can be understood in terms of the shower development. Earlier shower development means more nearly equal paths for detected particles, so they arrive more tightly bunched in time. The effect is accentuated for water detectors by the larger fraction of muon signal in the pulse since the muons undergo less scattering and arrive earlier, on average, than electromagnetic particles.

These three quantities – depth of maximum, muon density, and rise-time – are used in concert to determine the cosmic ray nuclear composition and to find the most likely mass for each primary particle. The hybrid data set will provide a distribution function on the 3-dimensional space (mu:em, $t_{10/50}$,$\hat{X}_{max}$). Here mu:em is the muon to electromagnetic density ratio at 1 km from the core,$t_{10/50}$ is the rise-time for pulses at that distance, and

$$\hat{X}_{max} \equiv X_{max} - \frac{d < X_{max} >}{d \log E}(\log E - \log E_0)$$

is the measured X_{max} corrected to a convenient reference energy E_0 using the observed *elongation rate* ($d < X_{max} > /d\log E$). Because the three measured parameters are correlated, the distribution function will be concentrated around a 1-dimensional curve in this space, where the curve can be parameterized by shower development speed. The observed distribution function on (mu:em, $t_{10/50}$, $\hat{X}_{max}$)-space will be compared with the expected distribution function for alternative composition hypotheses.

A potential difficulty is that the expected distribution function may also depend on untestable properties of hadronic interactions at the highest energies. It is conceivable that the composition determination could be hindered by inadequate knowledge of the first generations of hadronic interactions. It is likely, however, that the relevant interaction model parameters (e.g. energy dependence of cross section, inelasticity, and multiplicity) will be well enough constrained that ambiguities due to the model freedom will be small compared to differences expected from different composition hypotheses. Significant constraints on the hadronic model have been imposed by the Fly's Eye data[84]. HiRes and AGASA data can be expected to provide further constraints. By combining muon and electromagnetic particle measurements with X_{max} measurements, shower by shower, the Auger Observatory will provide valuable additional constraints. The Fly's Eye analyses have demonstrated that such data can be used both to constrain the interaction model and also to make composition inferences. In the Fly's Eye case, the model constraints derived from the need to explain the full range of the X_{max} distribution with nuclei of $1 \leq A \leq 56$. The energy dependence of the mean X_{max} was then used to infer a composition changing from heavy nuclei dominated to light nuclei dominated in the energy decade from $10^{18} - 10^{19}$ eV.

Above 10^{19} eV, γ-rays produce a characteristic signature due to the LPM effect [83]. This effect reduces the high energy electromagnetic cross sections, so the longitudinal profile becomes longer than that obtained using Bethe-Heitler cross sections. At Auger Observatory shower energies, a γ-ray shower is expected to have a significantly broader profile than any hadron-induced shower of equal energy, and the γ-ray showers should exhibit large fluctuations in X_{max}. The LPM effect grows with the γ-ray primary energy. The fluorescence detector's longitudinal profile measurements will enable a sensitive search for any γ-ray population.

At the time of writing, work on the multi-parameter composition sensitivity is still in progress. The composition resolution based on mu:em alone is exhibited in Figure 4.4. The resolution based on $\hat{X}_{max}$ alone is shown in Figure 4.5. Note that, in both cases, the air shower and detector response have been simulated with most relevant fluctuations. Changing the hadronic interaction model at the highest energies could change the locations of the peaks in those plots, but their separations should have little dependence on model variations[84].

4.2.4 New Particle Physics

Almost all the physics of air showers is well established. Electromagnetic sub-showers can be modeled with confidence. The majority of hadronic interactions in a shower can also be confidently modeled, since most interactions occur after many "branchings" of the shower,

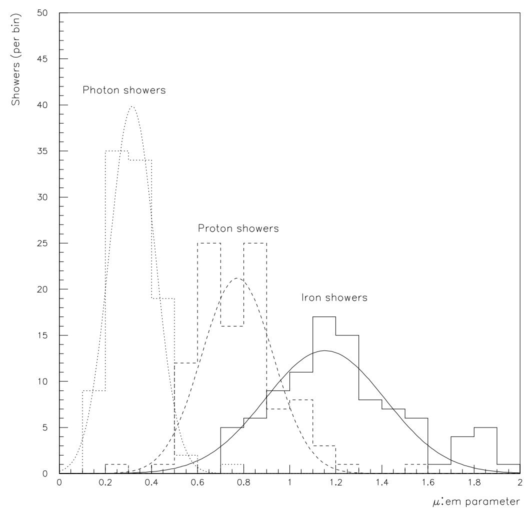

Figure 4.4: Predicted primary particle separation for the Auger surface array. Each distribution is from 100 showers at 5×10^{19} eV incident at 30°. The μ:em parameter is from reconstruction of realistically simulated detector signals.

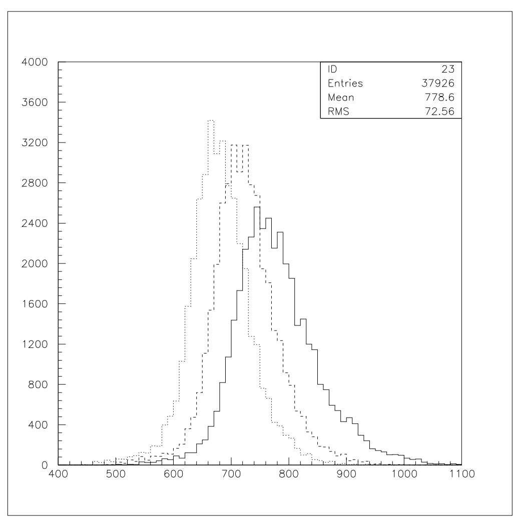

Figure 4.5: Reconstructed depth of maximum distributions from simulated iron (dotted histogram), carbon (dashed), and proton (solid) events. Showers up to 3×10^{19} eV are included, and all X_{max} values have been corrected by the elongation rate to a reference energy of 10^{18} eV. There are equal numbers of events in each histogram.

so individual particle energies are much reduced from that of the primary particle. Only the first few generations of interactions have center-of-mass energies greatly exceeding those of collisions studied in accelerator experiments. Collider experiments have explored hadronic interactions up to $\sqrt{s} = 2$ TeV. The Auger Observatory focuses on cosmic rays with energies above 10^{19} eV, for which the (nucleon- nucleon) center-of-mass energy is $\sqrt{s} = 140$ TeV.

Cosmic ray studies have a tradition of augmenting basic knowledge of particle physics. The Auger Observatory can expect to provide valuable information about particle interactions at a new frontier of energy. As happened with the Fly's Eye X_{max} distribution, combined measurements of mu:em, $t_{10/50}$, and $\hat{X}_{max}$ can be expected to constrain the interaction model even without independent knowledge of the composition. Measuring air showers provides not only information about the cosmic ray population (arrival direction patterns, energy spectrum, and composition), but offers a window to study new particle physics, if present.

Lack of complete *a priori* knowledge of hadronic interactions at the highest energies has only a limited impact on the Auger cosmic ray studies. The arrival directions can be measured completely independently of any model ambiguity. The electromagnetic shower energy is also measured without any reference to the hadronic model. It provides a solid lower bound for the cosmic ray's energy. The unmeasured energy is expected to correlate with shower development in a manner which is easily modeled. Composition studies cannot be totally divorced from models of the hadronic cascades' first few generations, but the relevant model parameters should be determined well enough to allow analysis of the mass distribution.

Systematic energy underestimation is possible if, for example, there is an unmodeled enhanced production of prompt muons which divert some of the total energy in the first interaction. Other uncertainty might arise due to the nonlinear behavior of QCD, which may cause intrinsic fluctuations in the numbers of particles produced in interactions ("intermittency")[85]. If either of these effects becomes very important at the highest energies, they may leave characteristic signatures in extensive air showers.

Learning how to model the highest energy interactions is vital for a comprehensive composition determination with the Auger data set. Developing and testing the interaction model will be a high priority of the Project. A meeting in conjunction with the Design Group Workshop was held at Fermilab in April 1995 to discuss the issues and set a course for future work. Efficient numerical simulation of air showers is an essential tool for designing the detector and evaluating its performance. The programs used for Auger are described in the next chapter.

4.3 Surface Array Methods

As described in the last chapter, most air shower experimental work has used surface arrays. Because of the low flux of extremely energetic cosmic rays, arrays require a very large collecting area (> 10 km^2) to collect a useful sample of events. The approach has historically been to cover the monitoring area, more or less uniformly, with a relatively small number (a few tens) of detectors, each having areas greater than about one square meter. A good example was shown in the last chapter, the Volcano Ranch array (Figure 3.1). In that experiment, the spacing between the 3.3 m^2 scintillators was 884 meters. At each detector of such an array the particle density is measured together with the arrival time of the signal at the detector relative to the other detectors. The geometry of the air shower is reconstructed from this data, the location of the densest part or "core" of the shower being determined under the assumption of circular symmetry (again, see Figure 3.1).

In the Volcano Ranch experiment the total number of particles in the shower was used to obtain the energy of the event. This total was estimated by integrating an empirically determined lateral distribution function (density *vs.* distance). The relationship between the number of particles and the primary energy was determined by invoking a detailed understanding of the physics of electromagnetic cascades. Modern air shower arrays use Monte Carlo calculations to relate the observed number of particles at ground level with the energy of the shower. The Auger ground arrays will use the inferred signal density at a specific core distance as their basic energy parameter. The reasoning behind this technique is described in sections 4.3.2 and 4.3.3 below.

The Volcano Ranch event also shows some other important features. Although the core of the shower impacts outside the geometrical boundary of the array it is well located by symmetry. Note also that significant signals are seen as far as 2.5 km from the shower axis. In the case of the Auger Observatory, due to its large size, it will not be necessary to use events which are not well contained within the array boundary.

4.3.1 Water Čerenkov lateral distribution function

Like the arrays planned for the Auger Observatories, the detectors of the Haverah Park experiment were water Čerenkov tanks (1.2 m deep and of various areas from 1 m^2 to 34 m^2) spread over 12 km^2: the array ran more or less continuously for twenty years. Much of the design information from the Monte Carlo calculations used by the Auger collaboration have been checked against results from this experiment (see section 5.2.4). A particular advantage of the deep water Čerenkov detectors lies in their ability to respond to the large number of photons of relatively low energy (less than 10 MeV) present in the shower. Empirical studies using unshielded and lead-covered scintillators and the water Čerenkov detectors, now confirmed by the Monte Carlo calculations, demonstrated that photons outnumbered electrons by about a factor 10 at the large distances of interest. The depth of the tanks, 3.4 radiation lengths, allowed conversion of the bulk of the photons so that electrons, photons and muons were recorded with high efficiency. The large area (4×13.5 m^2) of the detectors at the periphery of the array permitted densities to be measured as far as 3 km from the core in the largest events. The rise-times (10-50%) of the water Čerenkov signals were measured at four 34m^2 detectors which were on a 500 m grid at the center of the array.

The central element of the reconstruction and analysis of air showers using surface arrays involves fitting the lateral distribution function of particle densities. At Haverah

Park a good fit to the water Čerenkov lateral distribution was found to be the modified power law function:

$$\rho(r) = kr^{-\left(\eta + \frac{r}{4000}\right)}, \tag{4.1}$$

where shower core distance r is in meters, k is a normalization parameter, and η is given by

$$\eta = 3.49 - 1.29 \sec\theta + 0.165 \log\left(\frac{E}{10^{17}\ \mathrm{eV}}\right), \tag{4.2}$$

with θ the shower zenith angle, and E the shower energy.

The parameters η and k control the shape and normalization respectively. Representative values are $\eta \approx 2.5$ and $k \approx 3.5 \times 10^8$ for vertical 10^{19} eV showers. The signal density $\rho(r)$ is expressed here in units of vertical equivalent muons per square meter (VEM m^{-2}), obtained by dividing the total observed signal by the average value from a vertical through-going muon. Use of this density unit allows simple calibration of water Čerenkov detectors using background muons.

As shown by Equation 4.2 the slope parameter η is a function of zenith angle θ and, to a minor extent, shower energy. Both of these effects reflect the "aging" of a shower as it penetrates through the atmosphere. For four years 30 smaller water Čerenkov detector units also 1.2 m deep were operated in the central part of the Haverah Park array allowing detailed study of these effects and leading to Equation 4.2.

The lateral distribution shape given by Equations 4.1 and 4.2 is known to be valid for $50 < r < 800$ m, $\theta < 45°$ and $1 \times 10^{17} < E < 5 \times 10^{18}$. It was noticed that in the biggest showers, where measurements were recorded well beyond 800 m, there was a significant departure from this parametrization, the measured values of $\rho(r)$ being consistently higher. A special study of showers with $E \geq 1 \times 10^{19}$ eV indicated that these data were well represented by flattening the lateral distribution for $r > 800$ m. Thus, for the highest energy showers, Equation 4.1 is replaced at $r > 800$ m by the modified expression

$$\rho(r) = kr^{-\left(\eta + \frac{r}{4000}\right)} \left(\frac{r}{800}\right)^{1.03}. \tag{4.3}$$

Figure 4.6 shows four examples of actual Haverah Park data in this energy regime. Equations 4.1–4.3 are seen to do an excellent job of describing these data over the the entire measurement range. These events were experimentally very well measured. They fell close to an infilled part of the array so their cores are reliably located. This allows the lateral distribution at large distances to be observed with minimal reconstruction bias.

The flattening of the lateral distribution at large core distances seen in Figure 4.6 and expressed in Equation 4.3 can be understood in terms of a shift from an electromagnetic to a muon-dominated signal. It is a consequence of the broader muon lateral distribution which is predicted from simulation. The effect is enhanced in water Čerenkov detectors, where the higher energy muons release much more Čerenkov light per particle (recall Figure 4.2).

In Section 5.2.4 it is shown that current simulations do an excellent job of reproducing the empirical Haverah Park results. Since the Auger arrays are to be built at higher altitude than than Haverah Park (870 g/cm^2 as opposed to 1020 g/cm^2) it will be necessary to

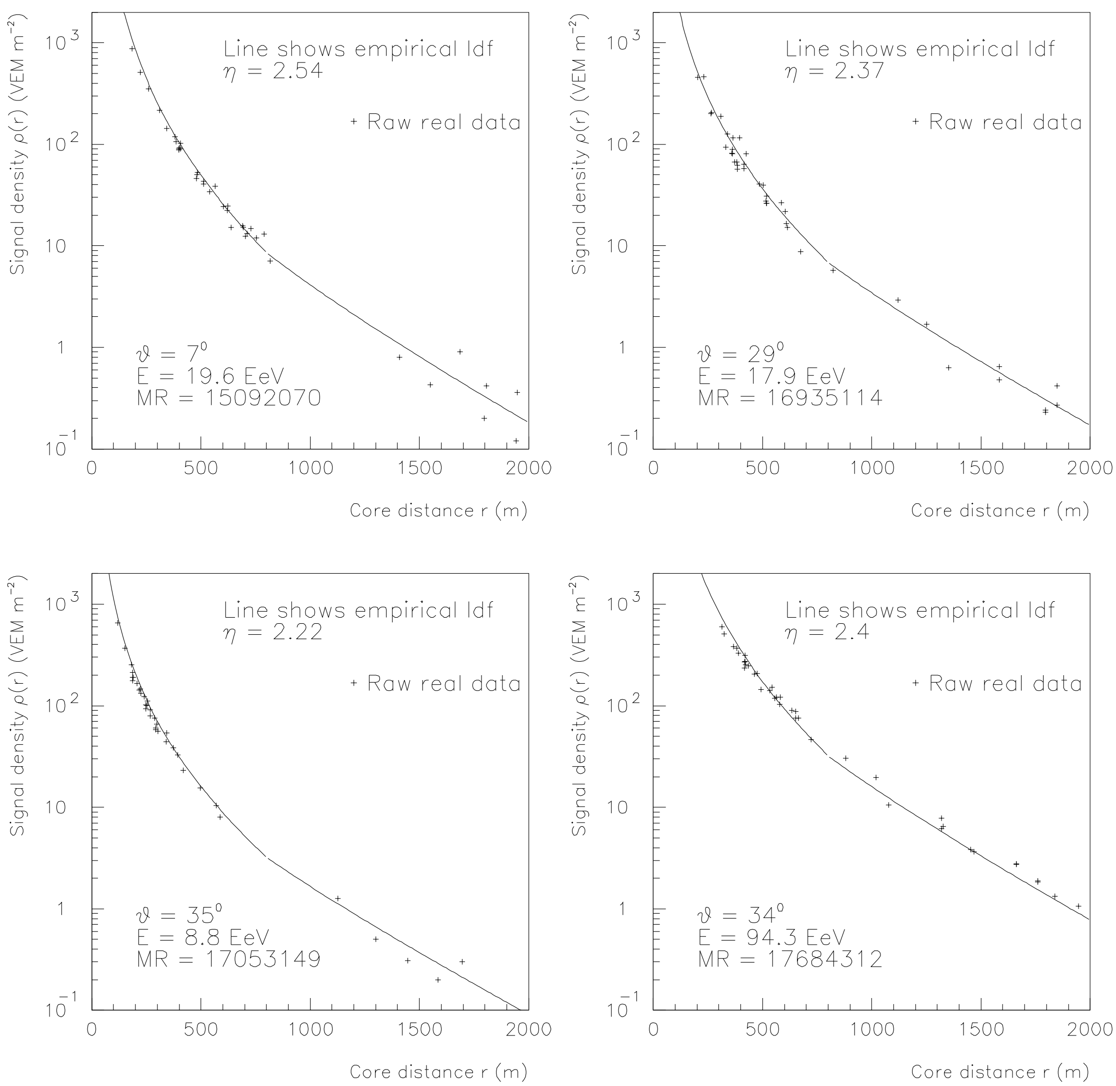

Figure 4.6: Haverah Park data showing four exceptionally well measured events at very high energy. The solid line is the lateral distribution function from Equations 4.1–4.3. The value of the slope parameter η is shown for each event, along with the best-fit values for energy and zenith angle; MR is an event identification code. Energy is expressed in units of EeV, where 1 EeV $= 10^{18}$ eV.

extrapolate the Haverah Park results, or more probably, to use an initial lateral distribution function derived from simulations validated using the Haverah Park results. Also, as mentioned in section 4.2.1, the Auger hybrid data set will allow independent investigation of the lateral distribution function.

4.3.2 Event Reconstruction

The structure of air showers was described in Section 4.1.2 above, and the reconstruction process briefly introduced in Section 4.2.1.

Figure 4.7 shows the reconstruction of an individual simulated event. The Haverah Park lateral distribution function was fit to the detector density measurements allowing the slope parameter η to go free in the last iteration. The 10% signal arrival time of the shower front (t_{10}) was fit assuming it to have a spherical shape in space; the radius of curvature was also allowed to go free at the last iteration. In time fits the observations are normally weighted by the corresponding detector densities. These two fits yield the shower incidence angles θ and ϕ, the core impact position, and the energy of the shower as inferred from the reconstructed signal at 1000 m from the core (see next section).

A final fit is illustrated; the shower front time dispersion ($t_{10/50}$) is analyzed on the assumption that it varies linearly with core distance. The slope of this fit, together with the lateral distribution slope parameter η, and the radius of curvature of t_{10} are sensitive to the mass of the primary particle.

It turns out that for a given array layout there is a distance at which the signal density is most accurately reconstructed. This results from a geometric effect whereby the errors in the determination of the lateral distribution slope and shower core position conspire to cancel at a given distance. The specific distance varies with shower impact position relative to the array grid, but it is on average somewhat less than the array spacing. For the Auger arrays it will be at $\approx$ 1 km. (For the Haverah Park array it was $\approx$ 600 m.) In the next section the proportionality between $\rho(1000)$ and the energy of the primary cosmic ray particle is investigated.

4.3.3 Energy Assignment Parameter

Air shower parameters scale in a well behaved manner with increasing primary energy. The best experimental demonstration of this has been provided by the series of arrays constructed at Akeno in Japan [123, 16]. Simulations also predict smooth scaling; Figure 4.8 shows the evolution of the lateral distribution over a broad range of energies.

The proportionality between the density observed at a given core distance and the energy of the shower changes with shower energy. This occurs because the shower is observed at differing stages of development as the depth of maximum increases with energy. In addition, the water Čerenkov detector's comparable sensitivity to muons and the electromagnetic component affects the proportionality of response as a function of radius. However, the evo-

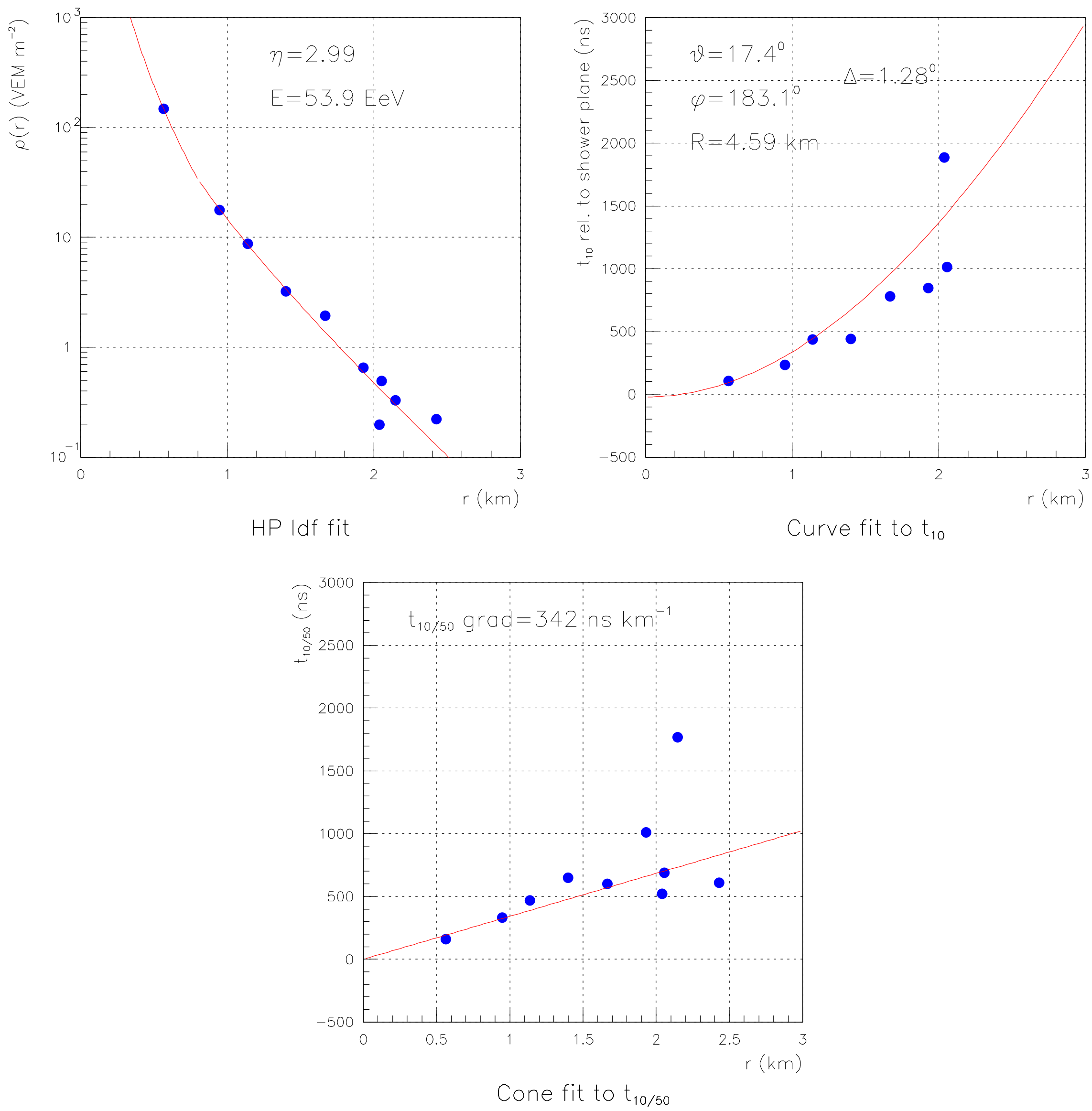

Figure 4.7: Reconstruction of a simulated Auger ground array event. At top right a lateral distribution fit to the Haverah Park functional form is shown; at upper right a fit to the 10% arrival time of the detector signals. The lower plot shows a fit to the shower front time dispersion.

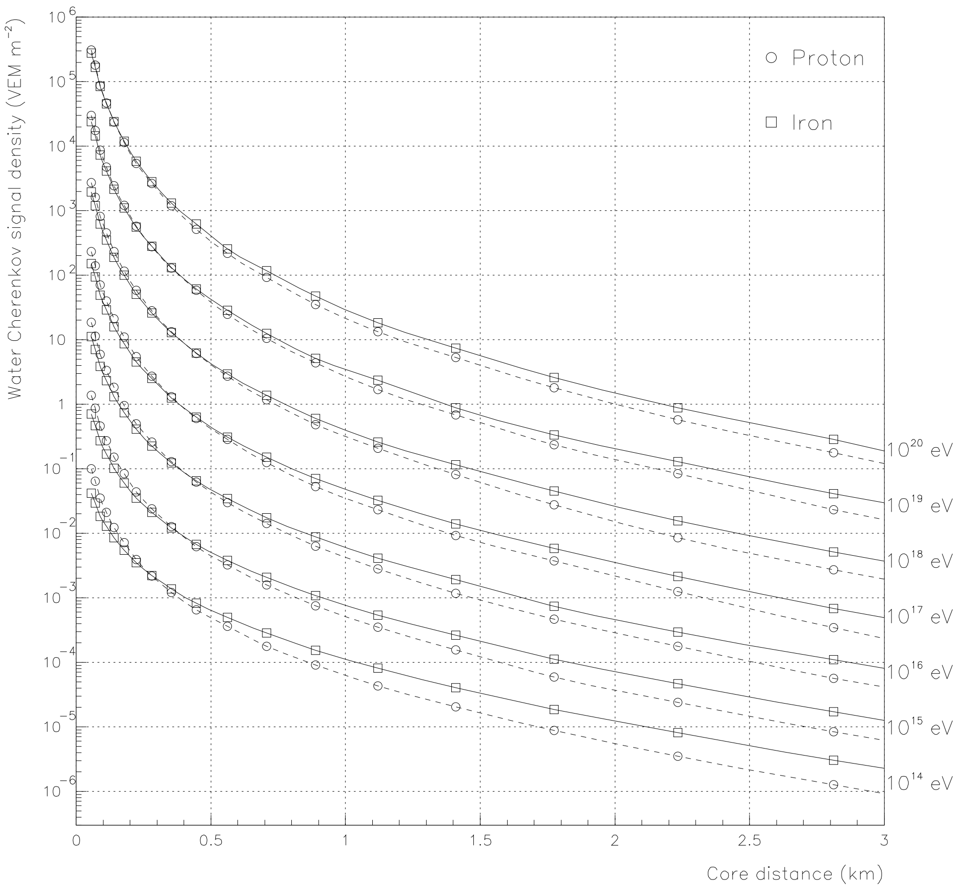

Figure 4.8: Simulated lateral distribution of air showers for a wide range of primary energies. The signal as observed in water Čerenkov detectors 1.2 m deep is plotted; calculation parameters are atmospheric depth of 850 g/cm^2, and zenith angle of 20°.

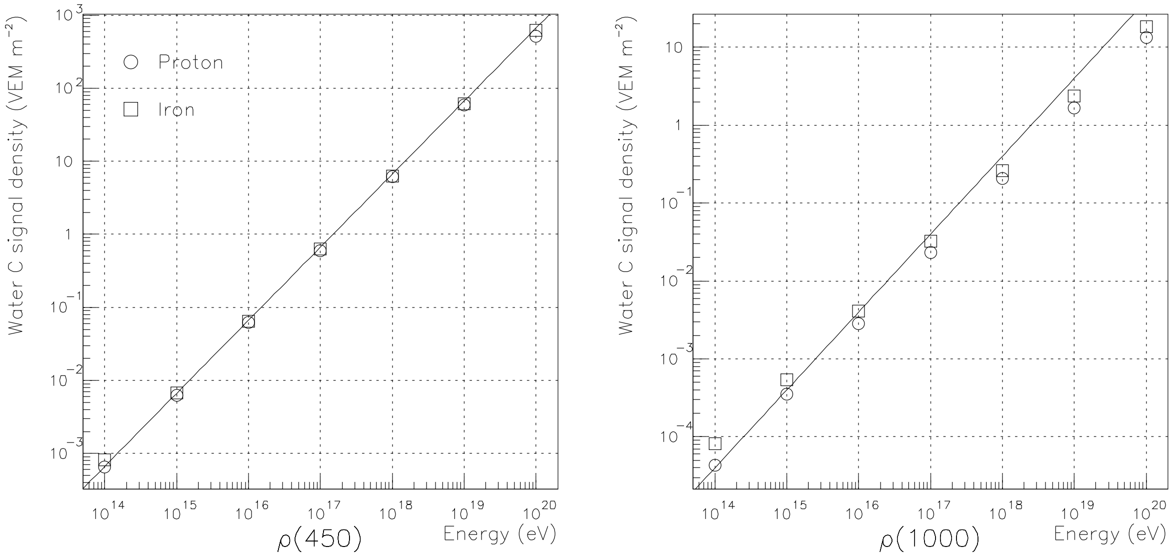

Figure 4.9: The signal density at two core distances plotted against air shower energy, and as observed by 1.2 m deep water Čerenkov detectors. Calculation parameters are atmospheric depth of 850 g/cm^2, and zenith angle of 20°. The solid lines show direct proportionality with the constant set such that the line passes through the proton point at 10^{14} eV.

lution of the lateral distribution with changing depth of maximum and muon content leads to very nearly proportional response at a particular core distance. Figure 4.9 shows the density versus energy at 450 m and 1 km. At 450 m the various factors give a density proportional to energy and nearly independent of composition. (Previous calculations by Hillas [114] found the same result at $\approx$ 500 m.)

Near 1 km there is both a slight deviation from proportionality and a modest dependence on composition. However, the Auger observatories will operate over a much narrower range of energies than shown in the figure; in the range $10^{18.5}$ eV to 10^{20} eV proportionality is good near 1 km. As discussed in the last section practicalities of ground array reconstruction dictate the use of the inferred signal density at $\approx$ 1 km as the minimum variance energy estimator. This implies some composition dependence for the energy assignment. However, as mentioned in section 4.2.2 above, it is expected that such dependence can be studied and reduced using the hybrid subset of the Auger data, and by separating the detector signal into electromagnetic and muonic components. More sophisticated methods than the simple energy parameter discussed here are under consideration.

4.4 Fluorescence Detection

The Auger Observatory is to be a hybrid detector. A giant array of particle counters will measure the lateral distribution of air shower particles at ground level. An optical component will measure the air shower longitudinal development in the atmosphere, using the technique established by the University of Utah's Fly's Eye detector. These atmospheric fluorescence measurements, although only available on clear, dark nights, will play an essential role by providing a subset of showers measured both laterally and longitudinally. This special subset will form the basis of the cosmic ray mass composition determination, as well as providing crucial cross-checks on the ground array's geometric reconstructions and energy determinations.

The primary role of the fluorescence detector is to measure the longitudinal profile of each shower. The integral of that profile is a direct measure of the shower's energy deposited in the atmosphere. The measured profile also yields information such as the atmospheric depth X_{max} at which the shower reaches its maximum number of secondary particles. For showers of fixed energy, X_{max} correlates with the mass of the primary particle.

It should be emphasized that the optical detector envisioned in this report has been designed to use ground array timing information to get good shower reconstruction capabilities. A fluorescence detector without a ground array, but with similar acceptance and reconstruction quality requirements, is considerably more expensive to build. Such a stand-alone fluorescence detector would need to view each shower simultaneously with two or more of its several eyes (i.e., in "stereo"). The intersection of the shower-detector planes from the different eyes gives the shower axis. To achieve two views of every shower for which we now plan one view would require either building twice as many separate eyes, or making each eye see twice as far. The cost of the fluorescence detector would be significantly increased, compared to the "monocular" design selected for the Auger Observatory.

4.4.1 Air Fluorescence

As a cosmic ray-induced particle cascade develops in the atmosphere it dissipates much of its energy by exciting and ionizing air molecules along its path. Excited nitrogen molecules fluoresce, producing near-UV radiation with an emission line spectrum as displayed in Figure 4.10. The efficiency of the process, defined as the radiated energy divided by the energy loss in the observed medium, is only $\sim 5 \times 10^{-5}$, but the vast number of emitting particles in a 10^{19} eV shower makes this source of radiation significant.

Fluorescence light is emitted isotropically with an intensity which is proportional to the number of charged particles in the shower. The number of fluorescence photons produced by N_e charged particles as they traverse a distance dl is expressed by

$$\frac{dN_\gamma}{dl} = N_f N_e,$$

where N_f is the fluorescent yield in photons/charged particle/meter. Strictly speaking, N_e should correspond to the total number of charged particles, but in practice it is often simply used to express the number of electrons and positrons since they so dominate the total number of charged air shower particles.

In practice N_f is very nearly a constant for most observational situations. As the pressure and temperature of the atmosphere is increased the excitation of molecular nitrogen is enhanced, but so is the probability of collisional de-exitation by oxygen molecules. The

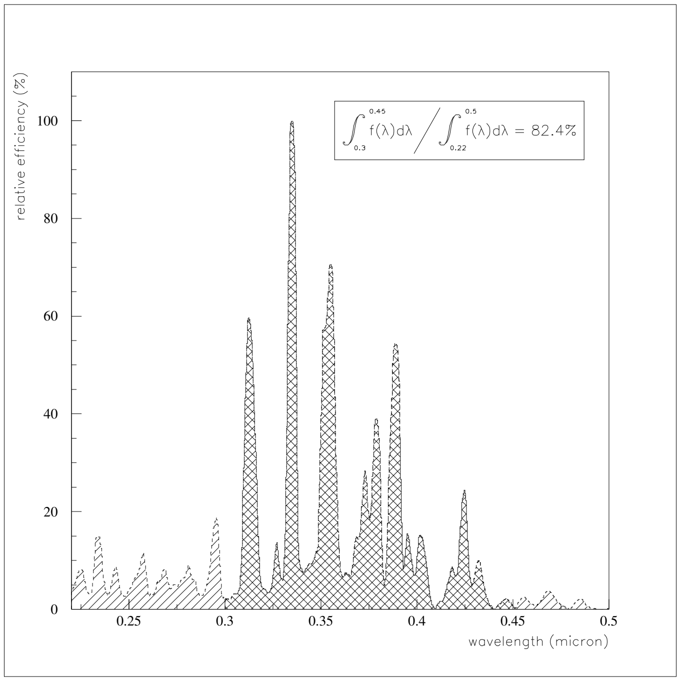

Figure 4.10: Emission spectrum of fluorescence light from the 2P band of molecular nitrogen and the 1N band of the N_2^+ molecular ion. Approximately 80% of the light is emitted between 300 and 450 nm.

two processes balance in such a manner that the variation in N_f as a function of altitude is quite small. Shown in Figure 4.11 are the results (for 80 MeV electrons) of an experiment in which a beam of electrons was sent through a chamber containing air at various pressures. The equivalent altitude is obtained using two standard atmospheric models. The observed fluorescence yield per meter of track length varies by less than 12% about an average of 4.8 photons/electron over a range of 20 km in effective altitude[108].

The relative constancy of the fluorescence yield greatly facilitates the use of this technique in which the number of particles at a given atmospheric depth is estimated via the amount of observed fluorescence light.

4.4.2 Čerenkov production and scattering

In addition to fluorescence light, showers produce prodigious numbers of Čerenkov photons which are primarily beamed in the forward direction. (The Čerenkov emission angle in the atmosphere is of order 1°, varying with altitude). The amount of Čerenkov light at a given point along the shower track depends upon the previous history of shower, and is thus not strictly proportional to the local shower size as is the fluorescent light. It is therefore necessary to estimate the amount of Čerenkov light in order to subtract its contribution to the observed signal. The number and angular distribution of Čerenkov photons over a

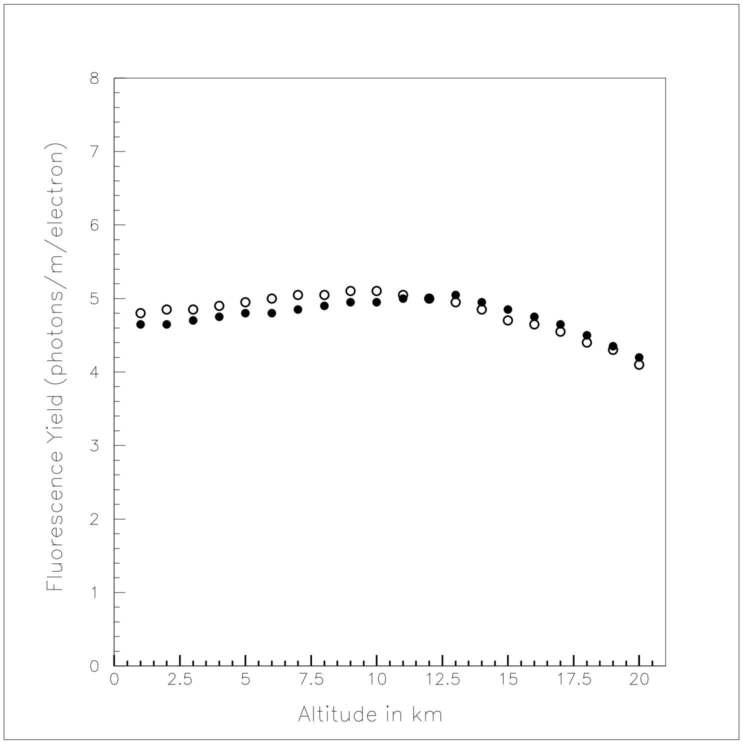

Figure 4.11: Air Fluorescence yields as a function of altitude. Open circles are for standard summer atmosphere while filled are for standard winter atmosphere[108].

distance dl of air can be approximated by :

$$\frac{d^2N_\gamma}{dl\,d\Omega} = \frac{dN_\gamma}{dl}\frac{e^{-\frac{\theta}{\theta_\circ}}}{2\pi\sin(\theta)}$$

where dN_γ/dl is the Čerenkov photon yield per meter of air, θ is the emission angle (in radians), $\theta_\circ = 0.83E_t^{-0.67}$, with E_t is the Čerenkov threshold energy in air in MeV. When a shower is viewed at small emission angles (less than 25°) with respect to the shower axis the Čerenkov signal can be many times larger than the fluorescence signal. The presence of this directly-beamed Čerenkov light often impedes the proper observation of the first stages of shower development. In addition, as the Čerenkov component builds up with the propagating shower-front, the resultant intense beam can generate enough scattered light at low altitudes such that it competes with the locally produced fluorescence light. This effect complicates the observations of the later stages of shower development.

Both fluorescence light and Čerenkov light are affected by the scattering properties of the atmosphere. The effects of scattering must be understood if one is to accurately estimate the shower size by light received from a distant section of air shower. With fluorescence light one is most concerned with the attenuation due to scattering as the light travels from the air shower to the detector. In the case of the (accumulated) Čerenkov beam, one is more concerned with the light scattered toward the detector. In both cases there are two scattering mechanisms: (1) Rayleigh (molecular) scattering and (2) Mie (aerosol) scattering.

The amount of molecular scattering at a given wavelength is proportional to the density of the air through which the beam is passing. The effect therefore tracks with the exponential

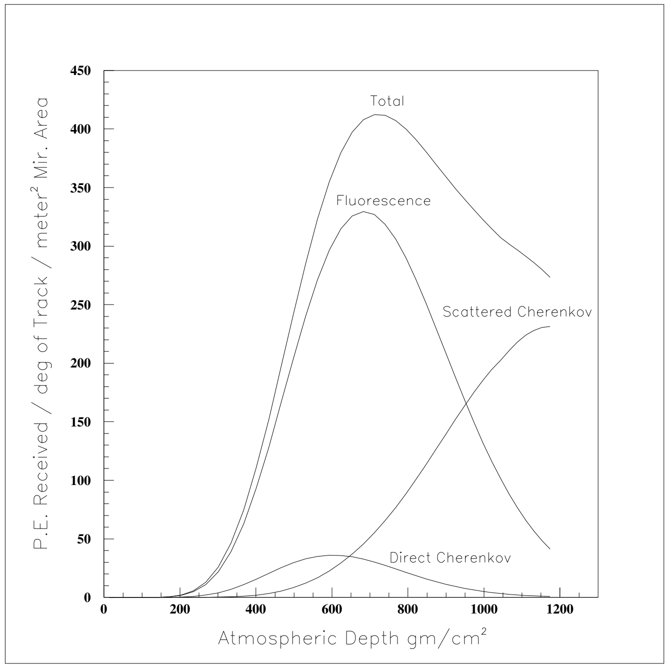

Figure 4.12: Estimated signal versus atmospheric depth of light production for a 10^{19} eV proton shower with orientation $\theta = 45°$,$\phi = 0°$ hitting the ground 10 km from the detector. The simulation included filters passing 300-400 nm light.

density profile of the atmosphere with a scale height of 7.3 km. In general the atmospheric density is well known and changes little over time. The Rayleigh scattering length at sea level is a constant 23 km at 400 nm. On the other hand, the degree of aerosol scattering depends on both the density and size distribution of particulate matter suspended in the air. These distributions are highly variable with time and location. For the desert atmosphere of the western United States the average aerosol scattering length is of order 10 km for wavelengths of interest in fluorescence detection. The vertical density distribution varies depending on weather conditions between an exponential form, similar to the molecular scattering situation and a distribution in which uniform scattering occurs beneath a fixed-height mixing layer.

Figure 4.12 illustrates the above ideas. The number of received photoelectrons versus atmospheric depth is plotted for a simulated 10^{19} eV shower at 10 km from the detector. This calculation includes the effects of 300-400 nm light filters on the apparatus. The total light, along with the contributions from fluorescence, direct Čerenkov, and scattered Čerenkov, are shown. The orientation and position of the shower has been chosen so that the contributions due to scattered and direct Čerenkov are enhanced.

This shower represents a worst-case situation for events which might be seen by the Auger Observatory near its energy threshold. The difference in the heights of peak emission of the fluorescence light and of the total light suggests that one would incur an error in energy of about 30% if the Čerenkov light contribution was ignored. The apparent shift of

50 g/cm^2 in X_{max} is significant however. Certainly, for highly inclined showers directed at the eye, both direct and scattered Čerenkov should be taken into account.

4.4.3 Detection Technique

An air fluorescence detector or "eye" consists of a series of large light collectors which image regions of the sky onto clusters of light sensing devices. The High Resolution Fly's Eye (HiRes) prototype detector [120] is an example of such a detector. In the following, it will be helpful to refer to this example.

HiRes uses fourteen f/1.16, 2-meter diameter spherical mirrors to collect the light from a 0.95 sr portion of the sky. The image plane of each mirror is populated with an array of 256 1-inch diameter (hexagonal) PMTs giving the instrument a 1° angular segmentation. The integrated charge and the trigger time are recorded for each PMT through which the shower image passes. The field of view of the mirrors is centered on the Chicago Air Shower Array (CASA) and the Michigan Muon Array (MIA) [121], situated 3.3 km to the northeast. The combination of the instruments has been used as a prototype hybrid detector where HiRes records the development profile, CASA records the ground particle density and MIA detects the muonic component of a common shower.

To a distant fluorescence detector a cosmic ray cascade appears as a rapidly moving spot of ultraviolet light describing a great circle path across a night-sky background of starlight, atmospheric airglow and man-made light pollution. The angular motion of the spot depends on both the distance and the orientation of the shower axis. The apparent brightness of the spot tracks with the instantaneous number of charged particles present in the shower but is also affected by Čerenkov contamination and atmospheric scattering as discussed above. The task of the optical detector is to pick out this faint, but fast signal from the ambient background noise, measure the shower trajectory from the appearance of the track and thelight arrival time as a function of the angular position, and to infer the shower development profile from the light flux from different parts of the track.

The shower track in the detector appears as long, rather narrow sequence of hit PMTs. The collection of vectors pointing from the PMTs defines a plane called the Shower Detector Plane (SDP). As the spot-like image of the shower proceeds through an individual PMT, the signal rises, levels off, and falls again. The transit time across the face of the PMT is given by

$$\Delta T \;=\; d\frac{R_p}{2c}\sec^2(\frac{\theta}{2}),$$

where R_p is the distance of closest approach between the detector and the shower track, θ (the viewing angle) is the between the PMT pointing direction and the shower axis in the SDP, and d is the angular width of the PMT's field of view. The physical length of track viewed by the PMT is $l \;=\; c\Delta T$. If the PMT aperture is circular and the shower path doesn't pass through the center of the pixel but misses by some fraction b of the pixel radius, then ΔT is further reduced by the factor $\sqrt{1-b^2}$. As an example, consider a vertical shower hitting the ground 10 km from the eye. A 1° pixel viewing the shower horizontally has a signal profile which is 523 ns wide. The pixel views about 175 meters of shower track and, at an operating altitude of 860 g/cm^2, that observed interval of track corresponds to a atmospheric depth interval of 20 g/cm^2 .

The magnitude S of the signal seen by a PMT depends on the size of the shower N_e, the distance R to the shower, the detector's sensitivity, and the time T over which the flux is collected. The relevant detector properties are the light collecting area A and the quantum efficiency ε. A is the effective area after correcting for mirror reflectivity and obscuration by the phototube camera at its focus. The signal S, in photoelectrons, is given by

$$S \ = \ 2.4 \ \frac{A\varepsilon N_e cT}{4\pi R^2} \ \xi(R),$$

where $\xi(R)$ characterizes the atmospheric attenuation and c is the speed of light. The fluorescence efficiency of the atmosphere in the frequency range appropriate to HiRes phototubes (with filters) gives the coefficient 2.4 photons/m per charged particle (so the above formula requires cT to be in meters).

The noise is governed by the background light from the night sky, which is approximately 40 photons/(m^2 deg$^2\mu$s) in the frequency range accepted by the HiRes filters and PMTs. [1] The noise is the square root of the background photoelectrons collected in T microseconds:

$$N \ = \ \sqrt{40\varepsilon A\Omega T}.$$

Here Ω is the pixel solid angle in square degrees.

The signal-to-noise ratio is therefore

$$S/N \ = \ \frac{2.4 N_e c}{4\pi R^2} \sqrt{\frac{\varepsilon AT}{40\Omega}} \ \xi(R).$$

Suppose the maximum of a vertical 10^{19} eV shower at $R = 10$ km is observed using the HiRes detector. Assuming an exponential atmospheric attenuation with attenuation length 10 km, a collection time $T = 0.5\mu$sec, and other parameters given above for the HiRes geometry, the S/N ratio for a HiRes PMT is about 9.1.

A practical detector must be able to accurately determine whether and when a shower image has passed through a given tube and thus call the tube "hit". In the case of the HiRes Prototype a tube is said to be hit when its RC filtered ($\tau_{RC} \sim 100$ ns) pulse height exceeds a voltage threshold which is continuously adjusted in response to changes in the background light level. The adjustments are made in such a way as to maintain a 200 Hz singles rate[2] in each tube. Signals which exceed this threshold correspond to a 4σ fluctuation in the background.

Even with this constraint, there will be tubes which report hits by chance. The detector must distinguish a random pattern of hit tubes from the pattern characteristic of a

[1] This is a representative value. The actual background intensity varies with elevation angle and atmospheric conditions. In normal running conditions, the background varies by less than a factor of two.

[2] This rate in the HiRes is about four times larger than the original Fly's Eye rate.

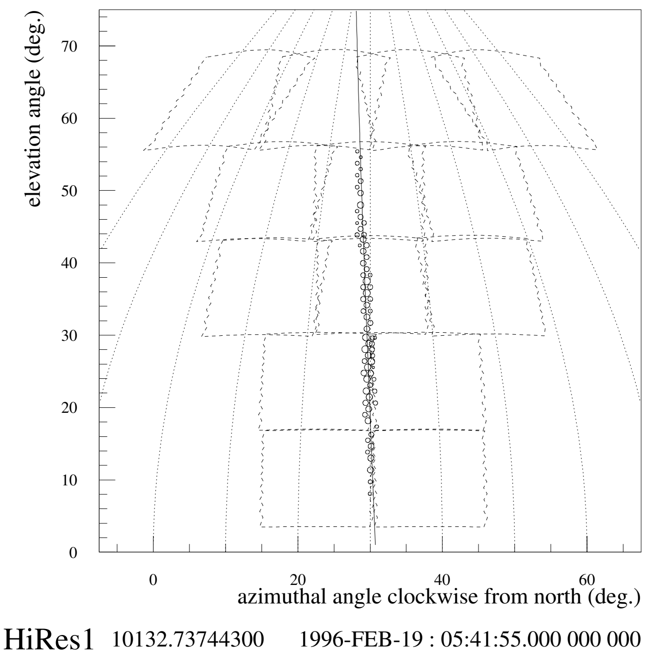

Figure 4.13: Typical HiRes shower, showing individual pixel hits and best-fit trajectory.

real shower. In addition, one must discriminate against showers that have geometries such that direct Čerenkov light dominates the fluorescence signal. Global triggering is a pattern recognition problem where the primary signature for the showers of interest is a linear pattern of hits which progresses in time. In the case of the HiRes prototype, each mirror (256 PMTs) can trigger independently. The cluster of tubes is arranged into 16 subclusters of 16 tubes(4×4). A hardware trigger occurs when at least 2 subclusters have at least 3 hit tubes, of which two of the three hit tubes are adjacent. The rate of these triggers is 0.5 - 1.0 Hz per mirror. Overall, the instrument triggers at about 10 Hz. Further discrimination criteria are implemented in software. Requiring a sensible angular velocity of the progression of hit PMTs reduces the rate of accepted ("real") fluorescent tracks to about 0.1 Hz.

For each triggered mirror, the detector electronics record and store quantities which are representative of the light flux as a function of time. The HiRes detector records the threshold crossing time to 25 nsec for each hit tube. It also records integrals of the signal over two time scales, 1.2 μsec and 5.0 μsec. Another technique which is still being developed by the HiRes group involves the use of signal digitization by flash ADC (FADC). In this technique the signal pulse profile can be digitized and recorded in its entirety. Figure 4.13 shows a typical shower as detected by the HiRes instrument. A spherical projection of the viewing regions of all 14 mirrors is shown with hit PMTs displayed as circles whose sizes are proportional to the number of photoelectrons collected. Noise hits, averaging only 0.5 per mirror per event, have been removed. The CASA and MIA detectors, which also saw this event, subtend a 5° azimuthal segment centered on 30°. This particular event will be used in the following discussions as an illustration of reconstruction techniques.

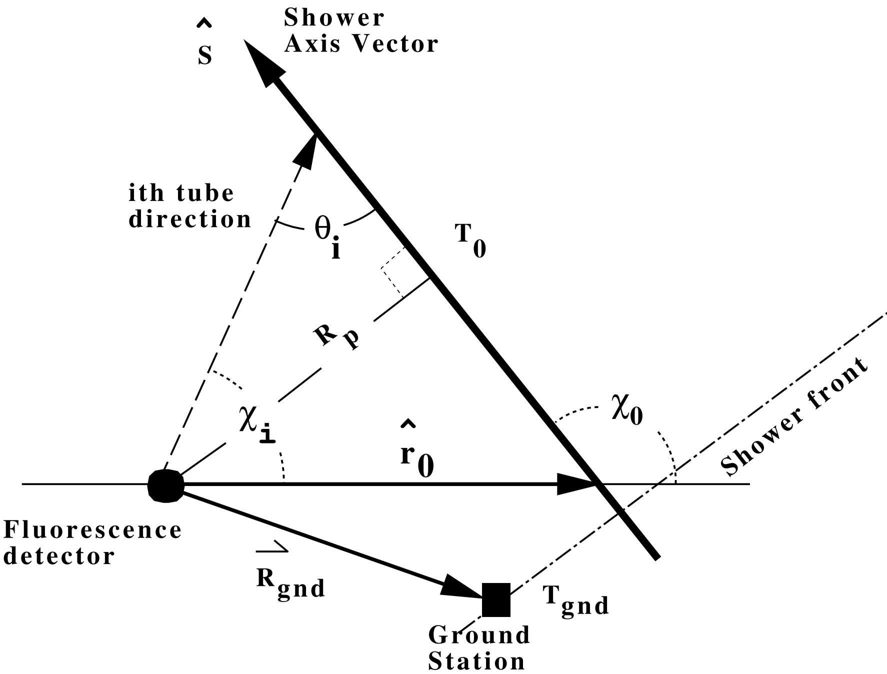

Figure 4.14: Shower/Detector Geometry.

4.4.4 Finding Shower Trajectories

The first stage in shower reconstruction is the determination of the shower trajectory. The process of trajectory finding occurs in two stages. First, the *shower-detector plane* (SDP) is determined[3]. The SDP is found using a fit to the eye's hit tube directions, where each point is weighted by the tube amplitude. The resulting plane normal vector can be determined in this manner with an accuracy of 0.2° [120]. The results of the SDP fit for the sample HiRes shower in Figure 4.13 is shown as a solid line through the hit tubes. The background (noise) tubes, about 0.5 per mirror, have been removed from this display.

In the second stage of track reconstruction the orientation and position of the shower axis within the SDP are determined. This amounts to finding the two quantities R_p and $\chi_\circ$ as defined in Figure 4.14. R_p is the impact parameter for the collision between the optical detector and the shower and $\chi_\circ$ is the angle in the SDP which the shower axis makes with the horizontal. Within the SDP the arrival time of light from the shower at each hit PMT is given by the following expression :

$$t_i = T_0 + \frac{R_p}{c} \tan\left(\frac{\chi_\circ - \chi_i}{2}\right),$$

where T_0 is the time at which the shower front passes closest to the eye (i.e., at distance R_p), χ_i is the ith PMT's elevation angle in the SDP, and c is the speed of light. The desired

[3]Note that the SDP is not the same as the shower front plane defined earlier, in Sec 4.1.2.

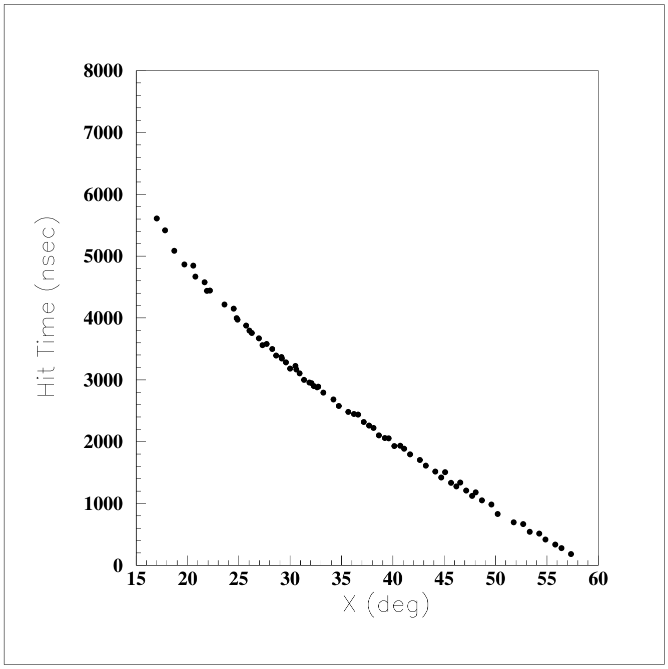

Figure 4.15: HiRes PMT hit time versus θ_i.

shower parameters may be found by minimizing :

$$\chi^2 = \sum_{i=1}^{N} \frac{(t_i - t_{obs_i})^2}{\sigma_i^2}$$

where t_{obs_i} is the observed tube trigger time and σ_i is the estimated measurement uncertainty in t_i.

When no ground array information is present the minimization is accomplished by varying three parameters R_p, $\chi_\circ$, and $T_\circ$. This procedure is often called the "mono" method of track reconstruction because it uses information from a single optical detector. In general there is a problem with this method, especially for tracks of short angular extent. The degree to which one can unambiguously determine more than two parameters in the fit depends on the degree to which the function $t_i(\chi - i)$ departs from linearity over the sampled range of angles χ_i. For most showers the range of sampled angles is small and $t_i(\chi_i)$ is indeed nearly linear. The situation is illustrated in the plot of observed PMT firing time t_{obs} versus χ for our sample HiRes shower in Figure 4.15. It is clear that for segments of track shorter than 20° very little curvature is detectable in the presence of the scatter of the points. Only two parameters are needed to describe the relationship between t_{obs} and χ for such segments, thus there is an ambiguity incurred when fitting for three parameters. This ambiguity can be resolved if information from the ground array is utilized in a hybrid fitting scheme.

There are two possible hybrid fitting schemes. In the first, the mono 3-parameter fit is replaced by a 2-parameter fit by specifying the angle χ_0 in terms of the shower direction derived independently by the ground array $\hat{S}_{gnd}$, through

$$\chi_0 = cos^{-1}(\hat{S}_{gnd} \cdot \hat{r}_0),$$

where $\hat{r}_0$ is the unit vector from the eye toward the shower impact point. In the case of our sample HiRes shower it was possible to use the shower direction, deduced from the arrival time distribution of the 665 detected muons, to constrain the fit. The shower landed 1583.7 ± 4.2 m East and $2653.9 \pm 7.1m$ North of the eye. The zenith angle of shower was $5.97°$.

In the second hybrid fitting scheme the reduction of fit parameters is accomplished by specifying the time T_0. T_0 can be calculated from the measured ground array trigger time T_{gnd} using

$$T_0 = T_{gnd} + \frac{\vec{R}_{gnd} \cdot \hat{S}}{c},$$

where $\vec{R}_{gnd}$ is the vector from the eye to the ground detector and $\hat{S}$ is the shower direction vector defined as pointing back along the shower path. In this expression it is assumed that the shower arrival front is planar. In real situations the shower front curvature must be taken into account. The hybrid Auger detector will use the latter method to determine shower trajectories.

We have reconstructed the geometry of our sample shower within the SDP in terms of R_p and χ_0 using the three methods just described. The results for each method and variable are presented along with the estimated statistical uncertainty in Table 4.1. The time T_{gnd} was obtained from a single 64-counter patch of the MIA detector which registered 56 out of a possible 61 hits. The estimated distance between this patch and the shower core is about 273 meters.

Fitting Method	R_p (meters)	$\chi_\circ$ (radians)
Mono	2981.1 ± 69.8	1.540 ± 0.044
Angle-Constrained	3089.6 ± 8.2	1.4739 ± 0.0028
Time-Constrained	3117.4 ± 6.4	1.4559 ± 0.0019

Table 4.1: Trajectory comparisons for a sample event using mono, time-constrained, and angle constrained fitting methods. All methods share a common shower detector plane so comparisons are made in terms of quantities R_p and χ_0.

4.4.5 Shower Shape and Energy

Once the trajectory has been found the next step is to use the PMT signal information to determine the shower size profile and total energy. In principle, a separate estimate of the shower size can be made by each tube seeing the track. A shower profile is then just a plot of these size determinations as a function of the particular atmospheric depth interval viewed by each tube.

If a tube views a linear interval of track l and receives N_{pe} photoelectrons while the shower was in view, then to a first approximation one can estimate the shower size N_e in

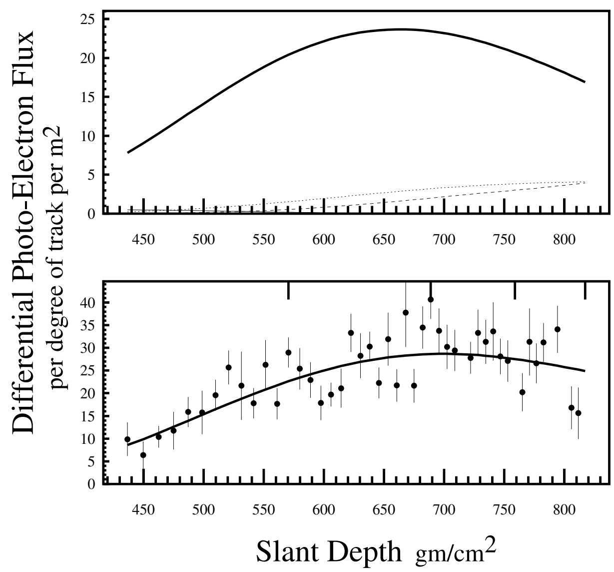

Figure 4.16: Observed light profile and the model estimate for a sample shower observed by the HiRes pototype detector. Lower plot is data with model superimposed. Upper plot is model decomposed into light production and scattering components.

the corresponding atmospheric depth interval by inverting the expression given above in section 4.4.3, to obtain

$$N_e = \frac{4\pi R^2 N_{pe}}{2.4 A\varepsilon l \xi(R)}.$$

In practice, the shower energy and size profile (and X_{max}) are found in an iterative process. First a model shower size profile is chosen, for example the Gaisser-Hillas [125] formulation

$$N_e \ = \ N_{max}(\frac{X - X_0}{X_{max} - X_0})^{\frac{X_{max}-X_0}{70}} \exp \frac{X_{max} - X}{70},$$

where N_{max} is the size at maximum and X_0 is the depth of first interaction. An initial guess for N_{max}, X_{max}, and X_0 is made. A received light profile is generated incorporating all known light generation and scattering processes. This profile is compared with the observations. N_{max}, X_{max}, and X_0 are then adjusted until the best agreement between generated light profile and observed light profile is reached. In Figure 4.16 the received light profile is shown for our example shower. Each data point in the lower plot is a measure of total light received per degree of track per square meter of mirror area at a given atmospheric depth. The solid line is the anticipated light received for a model shower which is in best agreement with the data. The upper plot shows what the model shower predicts for the contributions from fluorescence light (upper curve), molecular-scattered Čerenkov light (middle curve), and particulate-scattered Čerenkov light (lower curve).

At this point,the best-fit X_{max} has been obtained and the energy in the electromagnetic component is calculated by integrating the measured shower profile (as given in Sec. 3.2):

$$E_{em} = \frac{E_c}{\lambda_r} \int N_e(X)\, dX.$$

Our example shower has an estimated energy of $1.39 \pm 0.10 \times 10^{17}$ eV and a depth of maximum of 671 ± 16 g/cm^2.